Chemical Engineering Journal 101 (2004) 357–365

Chemical Engineering Journal

www.elsevier.com/locate/cej

Introduction of image analysis for the quantification of the boiling flow heat transfer

C. Ferret [a,*], L. Falk [a], U. D'Ortona [b], A. Chenu [a], T.T. Veenstra [c]

[a] *CNRS-LSGC-ENSIC, 1 rue Grandville, 54000 Nancy, France*
[b] *CNRS-LMSNM, 38 Rue Frederic Joliot Curie, 13451 Marseille Cedex 20, France*
[c] *MESA+ Research Institute, University of Twente, PO Box 217, 7500 AE Enschede, The Netherlands*

Received 31 July 2003; accepted 30 October 2003

Abstract

Heat transfer performances for non-boiling and boiling flow of a micro-vaporizer have been measured by standard methods (temperatures, flow rates, effective power input). The study was carried out for laminar flow ($Re < 25$) in silicon micro-channels (5 mm × 3 cm × 200 μm) filled with ordered obstacles to increase the specific area. The results obtained show a strong dependence of the heat transfer on the Reynolds number for the non-boiling flow and pretty high heat transfer coefficients (1300–2500 W/m^2 K) for the boiling flow. Image analysis was introduced to estimate the volume vapour fraction, which can be converted into the mass vapour fraction using the slip ratio. The estimation of this slip ratio is discussed in this paper.

Keywords: Heat transfer; Micro-structure; Laminar; Boiling; Image analysis

1. Introduction

This study deals with the performances of a micro-vaporizer realized in silicon and devoted to be a part of a micro-plant for hydrogen production [1] to supply a portable low power fuel cell (100 W). As the reactants (mixture of water and methanol) are fed in the liquid phase and the reactions in the reformer reactor take place in the gas phase, the first device of the micro-plant has to be a vaporizer. The required liquid flow rate to be vaporized is about 2 ml/min and the required exit temperature of the vaporizer is 260 °C (over heated vapour).

As the aim of the study is the miniaturization of the vaporizer, we investigated the field of micro-heat exchangers in laminar flow to both increase the residence time and reduce the pressure drop.

Advantages of micro-reactors and micro-heat exchangers are numerous (low volume and weight, high specific area, enhanced transfer coefficients, etc.) even if the pressure drops in this kind of structures is sensibly higher than standard devices. The main difficulty with such micro-systems is their accurate design because of the lack of heat and mass transfer correlations. Considering only the heat transfer in both single and two-phase flows, the trends observed in the literature are not all in agreement. Some authors report higher Nusselt numbers compared to standard (macro) ducts, whereas others report lower values. The results concerning the boiling flow do not agree either: the difference between the heat transfer coefficients presented by the various authors in micro-channels can reach a factor up to 5 [6,8].

Moreover, most of the researches presented have been carried out in the turbulent flow regime, with high pressure drops, whereas very few studies are reported for the laminar flow and almost no published data for really low Reynolds numbers (below 25).

In this paper the results concerning the single phase and boiling flow heat transfer coefficient measurements (without overheating) in a micro-heat exchanger are reported for pure water, and for several wall temperatures and flow rates. This exchanger has been realized by the powder blasting etching method in a silicon wafer, allowing the realization of very complex internal structures.

The volume vapour fraction at the outlet of the device has also been measured with an image analysis technique using a high-speed camera. Thanks to correlations determined for conventional ducts as detailed by Hewitt [2], it is possible to estimate the slip ratio between the liquid and

* Corresponding author.
E-mail addresses: ferret@ensic.inpl-nancy.fr (C. Ferret), falk@ensic.inpl-nancy.fr (L. Falk).

1385-8947/$ – see front matter © 2004 Elsevier B.V. All rights reserved.
doi:10.1016/j.cej.2003.10.028

Nomenclature

A	heating surface (m^2)
CHF	critical heat flux (W/m^2)
C_p	specific heat (J/kg K)
h	heat transfer coefficient (W/m^2 K)
ΔH_{vap}	vaporization heat (J/kg)
$\dot{M}$	mass flow rate (kg/m^3)
Nu	Nusselt number
Q	heat flux (W)
Re	Reynolds number
S	slip ratio (–)
T	temperature (°C)
X	mass vapour fraction (–)

Greek letters

α	volume vapour fraction (–)
θ_{TLM}	mean logarithmic temperature difference (°C)
ρ	density (kg/m^3)

Subscripts

in	inlet
out	outlet
exp	experimental
h	heating
boil	boiling
liq	liquid
sat	saturation
tl	thermal losses
tot	total
vap	vapour
w	wall

vapour phases to calculate the mass vapour fraction. This mass vapour fraction is then used for the heat balance and the determination of the heat transfer coefficient. The slip ratio can also be experimentally determined and will be compared to the values predicted using Hewitt relations. The validity of such correlation developed in macro-systems and applied to micro-systems will be discussed.

2. Experimental setup

The experimental setup (Fig. 1) is composed of a reservoir, a fluid circulation system (HPLC pump coupled to a pulse attenuator to ensure a constant flow rate), a 0.22 μm filter, the micro-structured plate thermally instrumented and heated on its whole surface via an electric resistance heater (DC) of power 100 W, and a condenser for the vapour.

The whole system is thermally insulated in order to minimize the thermal losses. A window in the insulator allows us to observe the micro-channel and to film the boiling flow behaviour. The high-speed camera is mounted on a two-dimensional displacement system to focus on the specific region of the flow.

The contact between the heater and the silicon plate is realized by thermal grease charged with copper particles to ensure a good heat transfer between the two devices (Fig. 2). The electric power input required to maintain the imposed temperature of the micro-channelled plate is measured. The inlet and outlet temperatures of the plate are measured as well as the wall temperature at four locations along the plate, using type K thermocouples of 500 μm diameter.

During the experiments on boiling flow a monochrome digital high-speed camera (256 × 256 pixels) was used to observe the behaviour of the two-phase flow at the outlet of the portion of the channel filled with obstacles. This camera was coupled to a video zoom to enlarge the portion of the channel observed and increase the accuracy of the view. Two cold halogen spots of 150 W were placed on each side of the camera to both avoid the presence of shadows inside the channels and to obtain a good image contrast. The typical size for the recorded images is 1.5 cm × 1.5 cm.

Depending on operating conditions of temperatures and flow rates, the rapid vaporization of the liquid can be observed. Vapour bubble bursts may then flush the liquid

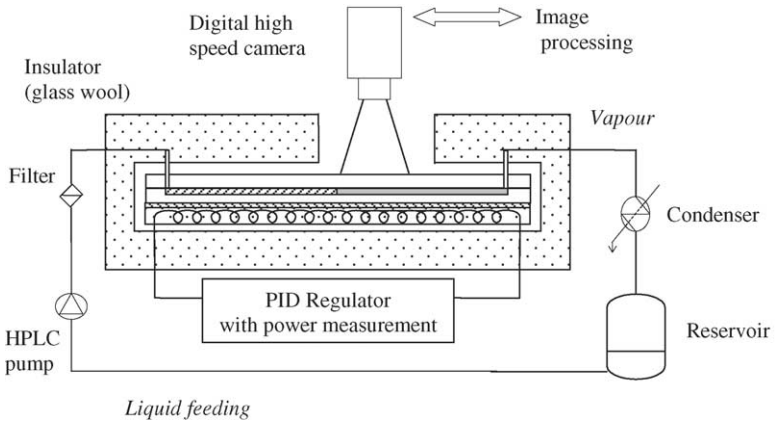

Fig. 1. Scheme of the experimental setup.

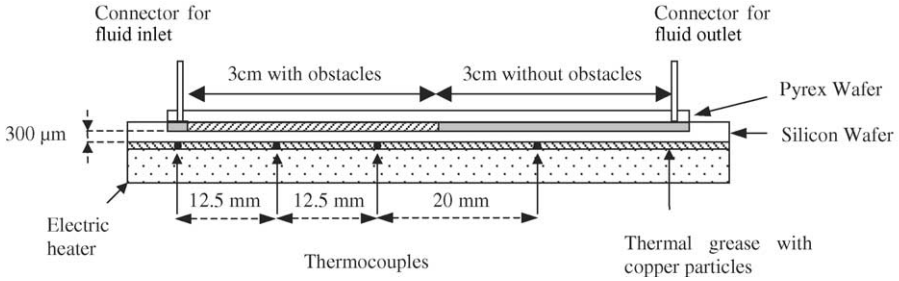

Fig. 2. Scheme of the heated silicon plate with thermocouples location.

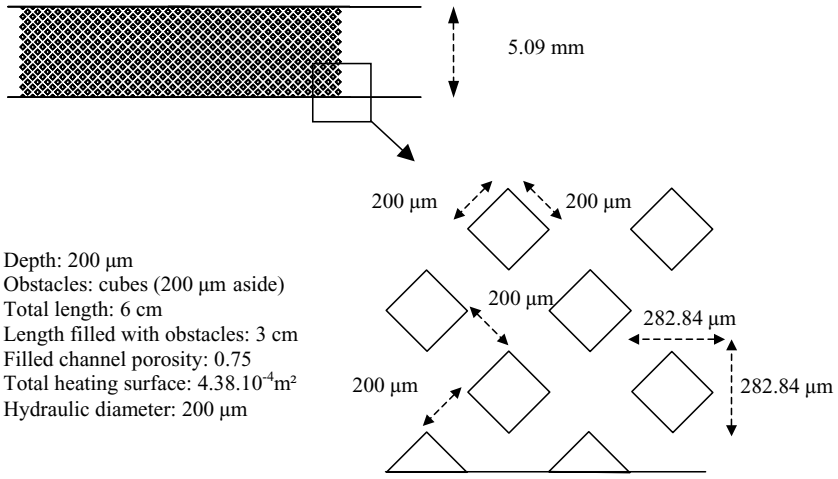

Fig. 3. Scheme of the micro-porous channel.

through the channel reducing the liquid–wall contact area and the residence time of the fluid, decreasing the overall heat transfer performance of the system. Therefore square obstacles are used (similar to an organized porous medium) in the chosen geometry to both increase the specific area and prevent the entrainment of liquid droplets. This kind of geometry is quite similar to the one presented by Brandner et al. [3] at the IMRET 4 conference, which showed very high heat transfer performances compared to straight channels.

The characteristic used to characterize the flow and heat transfer in the structure was defined to be the smallest dimension between the depth (200 μm) and the width (5 mm) of the flow cross section. In the present geometry the hydraulic diameter is then 200 μm.

These plates (Fig. 3) were realized by the MESA+ Research Institute at the University of Twente (Enschede, Netherlands).

The micro-channelled plate is made by assembling two different wafers (Fig. 4): one made of silicon in which the channels (200 μm depth) are etched by powder blasting through a polymer mask, and one made of pyrex to cover the first one [4,5] which allow the flow visualization. The absolute surface roughness of the obtained channels is below 2.5 μm.

The water used in the following experiments was obtained with a purification system which eliminates nearly all the ions present in the water, and filters the purified water on a membrane with 0.22 μm pores. The result is ultra pure water whose electric resistivity is 18.2 MΩ.

Even with such attention, previous experiments showed a strong fouling tendency of the system. This fouling has been identified to be mainly oxide deposition, due to the metallic connectors (Alumina) glued on the pyrex wafer for the exchanger liquid feeding.

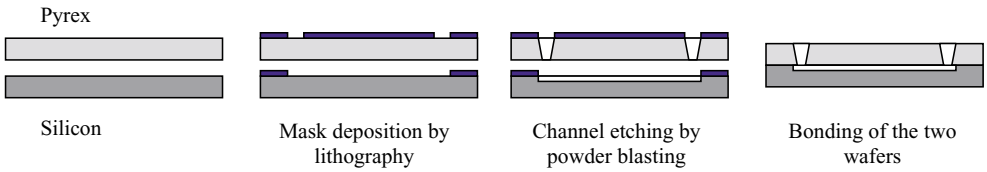

Fig. 4. Fabrication process of the micro-channelled plate.

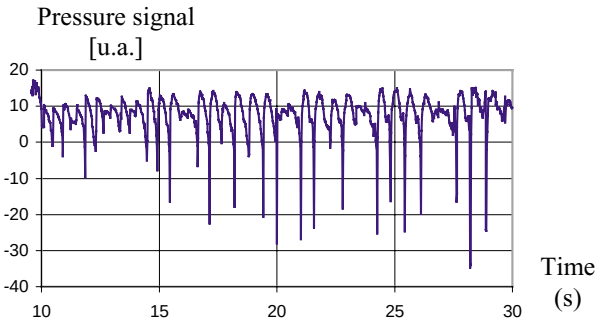

Fig. 5. Pressure drop signal in time for a flow rate of 0.6 ml/min and a wall temperature of 110 °C.

The formation of bubbles, under boiling flow conditions, is an unstable process (Fig. 5), even if the thermal equilibrium is reached. The main difficulty encountered at this step was to obtain representative images of the flow, and especially of the volume vapour fraction. Fig. 5 shows the pressure drop in arbitrary unities in time under boiling conditions of pure water and a wall temperature regulated at 110 °C.

The quasi cyclic pressure variations (period 0.6 s) correspond to the exhaust of a vapour bubble from the channel, leading to a non-constant volume vapour fraction in the channel. To take into account the time variation of the volume fraction, we decided to use a high-speed camera with a constant speed of 200 fps with an aperture time of 0.002 s. This frequency, much higher than the pressure drop frequency, allowed us to capture all the vapour volume variation during each cycle with a decent image processing time. The total duration of the film was limited to 10 s, corresponding to 2000 photos. A time of 4 h, was needed for each experiment to reach the steady state before realizing the measurements.

3. Heat transfer measurements

3.1. Experimental method for the heat transfer coefficient measure

The electric heat flux Q_{tot} supplied to the system to maintain the temperature at constant value can be divided into three terms: one for the thermal losses to the environment (Q_{tl}), one for the effective heat flux to heat the liquid up to its saturation temperature (Q_h) and the last one to perform the liquid vaporization (Q_{boil}):

$$Q_{tot} = Q_{tl} + Q_h + Q_{boil} \quad (1)$$

The thermal losses term (Q_{tl}) can be determined experimentally by measuring the power required to maintain the plate to the desired temperature without any fluid circulation. As we worked with an imposed wall temperature, the thermal losses are supposed to remain constant as long as the wall temperature is constant, independently of a liquid circulation or not.

During all the experiments, the ratio of the total power supplied to the power lost to the environment was within the range 60–70%. So only 30–40% of the total heat supplied to the system was effectively transferred to the liquid, even with 5 cm of a good insulation of the whole system (glass wool). The difficulty encountered here is the very low flow rate which induces a low thermal power transferred to the liquid, which is of the same order of the thermal losses.

The heat flux corresponding to the heating up of the liquid (Q_h) is calculated using Eq. (2). This second term can be measured during experiments carried out without phase change (single phase heat transfer).

$$Q_h = \dot{M} C_p (T_{out} - T_{in}) \quad (2)$$

In the case of boiling flow experiments, we have assumed that the liquid was heated up to its boiling temperature in the inlet distribution chamber, and then enters the micro-structured channel at its saturation temperature (i.e. $T_{out} = T_{sat}$ in Eq. (2)). This assumption has been checked successfully by CFD calculations.

During all the experiments, the highest temperature difference observed between the four measurement positions along the channel was 2.7 °C for a wall temperature of 80 °C. So assuming a constant wall temperature seems reasonable, but it also introduces a maximal error of 3.4% on the wall temperature.

The heat flux corresponding to the vaporization heat Q_{boil} can then be estimated by the difference between the electric power supplied and both the thermal losses and the power required to heat the liquid up to its boiling temperature (Eqs. (1) and (2)). The boiling heat transfer coefficient and the mass vapour fraction (X) can then be deduced from Eq. (3) for each experiment.

$$Q_{boil} = \dot{M} X \Delta H_{vap} = h_{boil} A (T_w - T_{sat}) \quad (3)$$

3.2. Definitions used for the calculation of Reynolds and Nusselt numbers

The characteristic length used to calculate both the Reynolds and the Nusselt numbers in the present paper is the one which induces the confinement to the system, i.e. the smallest dimension between the channel's width and depth, i.e. 200 μm. The physical properties of the fluid (density, viscosity, etc.) have been calculated at the average temperature between the inlet and the outlet for the single phase heat transfer. For boiling conditions, these properties have been calculated at the saturation temperature.

The liquid velocity which has been considered is the mean fluid velocity inside the micro-structure, estimated by the ratio of the flow rate divided by the mean open section for the circulation.

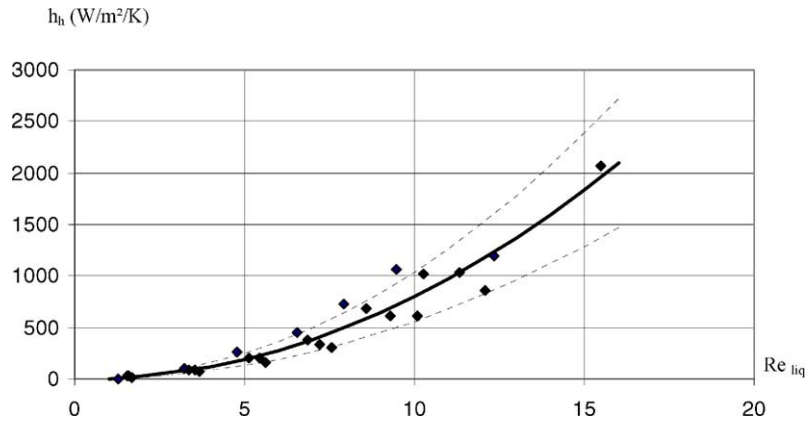

Fig. 6. Dependence of the heat transfer coefficient on the liquid Reynolds number.

3.3. Single phase heat transfer

The first experiments carried out were to investigate the single phase heat transfer coefficient by measuring the inlet and outlet fluid temperatures, as well as the wall temperature.

The conditions tested for the single phase heat transfer are the following:

- flow rate: 4.2×10^{-9} to $33 \times 10^{-9}\,m^3/s$;
- wall temperature: 55–95 °C.

Then using Eqs. (2) and (4) we can calculate the experimental value of the overall heat transfer coefficient h_h.

$$Q_h = h_h A \theta_{TLM} \quad (4)$$

The mean logarithmic temperature difference is here used to take into account the liquid temperature rising because of the non-linear profile of the liquid temperature in the exchanger. The results obtained are presented in Fig. 6.

In Fig. 6, we can observe the influence of the Reynolds number on the heat transfer coefficient which can be represented by a power law (Eq. (5)):

$$h_h = 6.96 Re^{2.0} \quad (5)$$

This power law allows us to predict about 85% of the experimental data, with accuracy of about 70%. The dash lines correspond to an error of ±30%.

This influence of the Reynolds number is in agreement with the phenomena observed by other authors, as Wu [6] or Peng [7], in linear channels even if the power observed here is higher (Fig. 7). The observed powers on the Reynolds number are 0.946 for Wu and 0.620 for Peng, who both studied straight channels with different aspect ratios.

The main difference between the experiments presented in this study and the results presented by Wu and Peng is the type of geometry used. Peng worked on straight channels made of stainless steel with rectangular cross sections of different aspect ratio ($0.15\,mm < D_h < 0.343\,mm$), whereas Wu used trapezoidal micro-channels made in silicon.

The experimental values obtained at $Re = 10$–20 are in good agreement with data published by Peng and co-workers.

Very few data in structures similar to porous media are available and are even less for very low flow rate in such structures. The closest studies are the ones made by Brandner et al. [3] and Tanda [9], which were both realized in micro-structured channels with respectively hydraulic

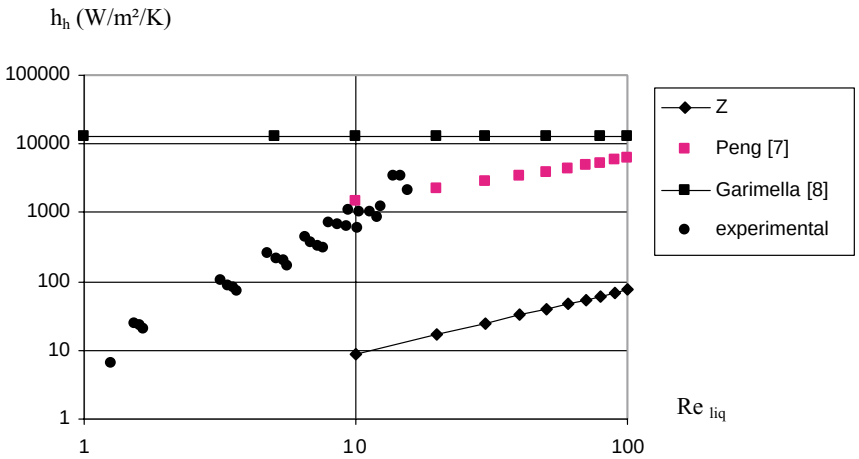

Fig. 7. Comparison of the experimental single phase heat transfer coefficient with the literature data for laminar flow regime.

diameters of 133.3 and 33 μm, with various organized type of obstacles for Tanda. They observed enhanced heat transfer coefficients for channels using a structure close to a porous media, compared to straight channels: for Brandner, the augmentation was up to 2.5 times, whereas for Tanda, it only reached a maximum of 1.6 times the heat transfer coefficient obtained for straight channels.

However, these studies have been carried out for much higher Reynolds number (Brandner: $Re > 1500$; Tanda: $Re > 5000$) corresponding to the turbulent regime and cannot be compared directly to our results.

In our case, the high influence of the Reynolds number can also be attributed to the specific geometry, which may induce mixing effects due to recirculation and backflows behind the obstacles.

3.4. Boiling flow

The conditions tested for the boiling heat transfer are the following:

- flow rate: 8×10^{-9} to 25^{-9} m^3/s;
- total heat flux imposed: 50–95 W.

The experimental boiling heat transfer coefficients obtained by the measure of the electric power supplied to the system (Eqs. (1)–(3)) can be presented as a function of the mass vapour fraction (Fig. 8).

The heat transfer coefficients obtained for boiling conditions are of the same order of magnitude as the single phase heat transfer coefficients. This figure shows the relative little influence of the mass vapour fraction on the heat transfer coefficient in the range 0.1–0.7: the mean relevant power on the mass vapour fraction was calculated to be about −0.18 on the whole range of X.

$$h_{\text{boil}} = 1452X^{-0.18}$$

This trend is close to the results obtained by Agostini [10] for mass vapour fractions above 0.19, who found the heat transfer to be reduced by increasing mass vapour fractions, but with a power around −0.55 for Reynolds number ranging from 0 to 2200.

This difference can be attributed to the different geometries used in the two studies: Agostini used a single straight channel with a hydraulic diameter of 0.77 mm, whereas our testing device consists of a wide channel filled with obstacles.

Our specific geometry is designed to favour the contact between the liquid and the wall by catching the liquid droplets carried along by the vapour on the obstacles. This design increases therefore the liquid/wall contact area. The droplets can then be vaporized faster, and the effect is a reduced influence of the mass vapour fraction.

The quantitative comparison of our experimental heat transfer coefficients to the values predicted by the relation of Agostini shows lower heat transfer coefficients for mass vapour fractions below 0.6. This observation has not been explained yet, but we can suggest the effect of the higher heat flux densities in the present study (up to 70 kW/m^2 against 31 kW/m^2 for Agostini). These higher heat flux densities could induce the formation of a vapour blanket between the wall and the liquid and then increase the thermal resistance of the system.

The experimental heat transfer coefficients have been plotted in Fig. 9 as a function of the Reynolds number at the inlet of the vaporizer (liquid conditions), and two domains with different behaviours can be noticed. At Reynolds values lower than 12, the heat transfer coefficient is a function of the Reynolds number, whereas at Reynolds above 15, there is almost no dependency of the flow on the heat transfer.

The heat transfer coefficients presented in Fig. 9 are way lower than those obtained by Peng [11] for pure water (6000 W/m^2 K) in tubes with hydraulic diameter of 150 μm and a wall temperature of 130 °C. Such a difference has not been explained yet, even if Peng results were obtained for Reynolds number above 140.

Moreover, the heat transfer coefficient appears to be influenced by the wall temperature, whatever the Reynolds number. The trend observed here is a lower heat transfer

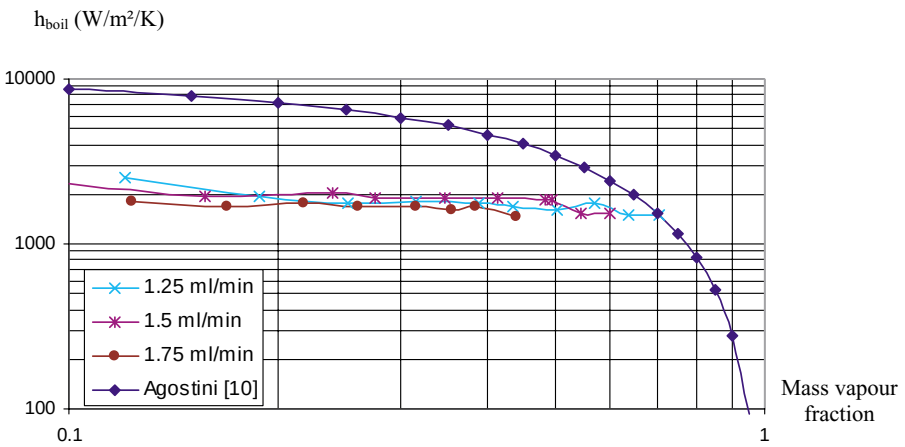

Fig. 8. Boiling flow heat transfer coefficients versus the mass vapour fraction for different liquid flow rates (in ml/min).

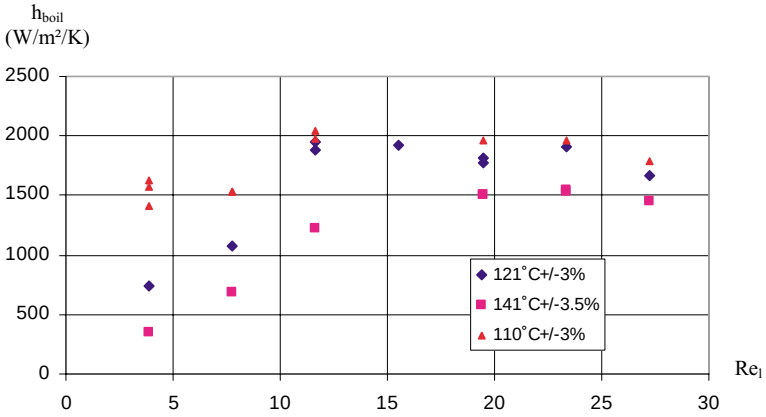

Fig. 9. Boiling heat transfer coefficient versus the liquid Reynolds number for two wall temperatures.

coefficient at higher wall temperatures, meaning an increased thermal resistance, which may be due to calefaction effect on the wall. This phenomenon has been previously detailed by various authors (Stephan [12], Rohsenow [13]) and is described as the apparition of a vapour blanket formed between the wall and the boiling liquid, which increases the thermal resistance of the system and thus reduces substantially the overall heat transfer coefficient.

4. Image analysis

4.1. Estimation of the volume vapour fraction

The use of the camera allowed us to realize images on which different area could be observed, corresponding to different behaviour of the liquid. These behaviours could then be related to different grey scale ranges.

This grey scale range was observed to depend on the type of contact between the water and the two walls, silicon and pyrex (Fig. 11).

In Figs. 10 and 11 it can be noticed that in the case of a dry channel, the channel appears as light grey (A). The dark grey regions correspond to both a channel fully wetted (B) and a channel partially wetted, water droplets only wetting the silicon wall (C). The difference between cases (A) and (B) is the presence of a dark boundary which corresponds in case (B) to the liquid/vapour interface. The last behaviour (D) is a channel partially wetted, the water droplets only wetting the glass wall, which corresponds to a nearly white grey scale range.

A different grey scale range (within 0 and 255) could then be attributed to each behaviour to distinguish them from each other (Table 1).

These data were used to write a program using Visilog 5.4 which sorts each pixel of the recorded images and decides

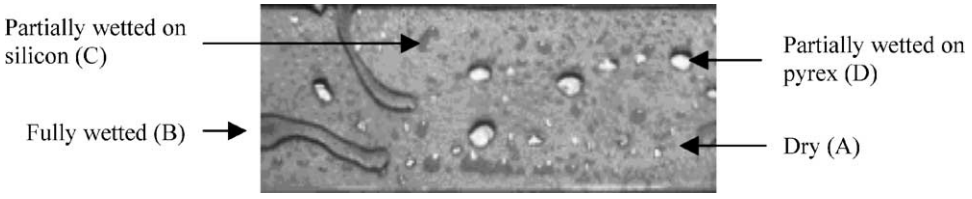

Fig. 10. Water liquid droplets deposition in the micro-channel.

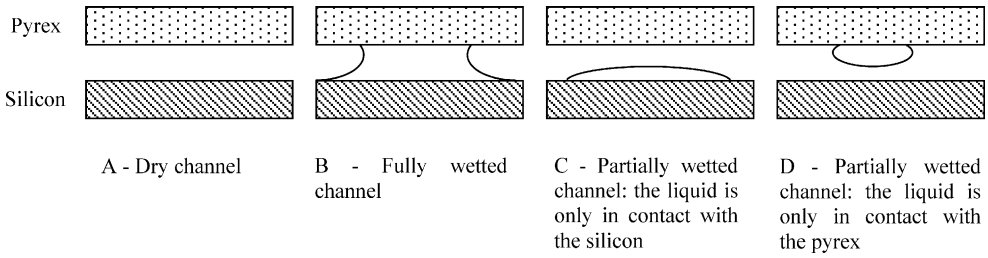

Fig. 11. The different behaviours of the liquid phase observed by image analysis.

Table 1
Grey scales ranges corresponding to Figs. 9 and 10

Behaviour	A	B	C	D
Grey scale range	80–240	0–80	0–80	240–255

whether it belongs to the liquid or the vapour phase (Fig. 10), depending on the grey scale of the pixel. This grey scale thresholding was chosen because of its ease of application compared with an edge detection algorithm. Moreover, the results accuracy is comparable between the two methods (below 2%) if particular attention is paid to the plate illumination.

We can thus estimate the fraction of the vapour phase to the total number of pixels in the channel, which correspond to the surface volume fraction. We then assumed this fraction to be equal to the volume vapour fraction because of the very small depth of the system. This assumption leads us to overestimate the liquid volume fraction.

4.2. Measure of the mass vapour fraction

The aim of images processing is to measure the vapour mass fraction X to estimate the heat transfer coefficient without any temperature measurements (as the total electric power supply measurement). The only requirement is to first realize a calibration of the thermal losses, depending on the temperature of the surrounding and of the device. The heat balance (Eq. (3)) can easily be established between the heat flux transferred from the wall to the liquid, which is supplied to perform a partial vaporization.

However, the mass vapour fraction is not directly accessible from image analysis, and only the volume vapour fraction α can be measured. This measured volume vapour fraction cannot directly be converted into the mass vapour fraction because the liquid and the vapour do not flow at the same velocity [2,14]. We then need to use the ratio of the vapour to the liquid velocities to calculate the mass vapour fraction. This slip ratio (S) can be calculated by two ways: an experimental method and a correlative method described by Hewitt.

The experimental slip ratios have been calculated from our experimental data using Eq. (6) where the mass vapour fraction X is determined from heat balance (Eq. (3)) and the volume vapour fraction α is measured by image analysis (Fig. 12).

$$S = \frac{1}{(1/X - 1)(\rho_{vap}\alpha/\rho_{liq}(1-\alpha))} \tag{6}$$

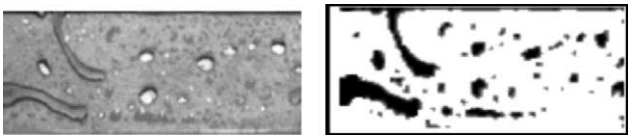

Fig. 12. Typical image for the estimation of the volume vapour fraction, before (left) and after image analysis (right).

These experimental slip ratios could then be compared to the values predicted by the relations (7)–(10) proposed by Hewitt [2]. However these correlations were developed in non-boiling conditions (air and water for large tubes).

$$S = 1 + E_1\left(\frac{y}{1+yE_2} - yE_2\right)^{0.5} \tag{7}$$

With the following expressions for the parameters E_1, E_2:

$$E_1 = 1.578\, Re_{liq}^{-0.19}\left(\frac{\rho_{liq}}{\rho_{vap}}\right)^{0.22} \tag{8}$$

$$E_2 = 0.0273\, We_{liq}\, Re_{liq}^{-0.51}\left(\frac{\rho_{liq}}{\rho_{vap}}\right)^{-0.08} \tag{9}$$

With the Weber number defined for the liquid flow at saturation temperature:

$$We = \frac{U_{liq}^2 \rho_{liq} D_h}{\sigma}$$

y is defined as the ratio of the volume vapour flow to the volume liquid flow:

$$y = \frac{(1-\alpha)S}{\alpha} \tag{10}$$

The calculation method is iterative and requires estimating the value of S, an a priori value of S to calculate the parameters y, E_1 and E_2 to be introduced in Eq. (8) to give a new value of S. If the recalculated value is different from the estimation, a new iteration is performed with another value of S.

4.3. Comparison of experimental and correlative results

Table 2 compares the values of both the slip ratios calculated from the experiments and using the correlation proposed by Hewitt for a liquid flow rate of 1.5 ml/min.

We can observe a strong discrepancy between the values of the slip ratios calculated from the experiments and the ones predicted by the Hewitt's correlation. Several explanations can be given to explain such a discrepancy: the assumption made previously about the equality between the

Table 2
Comparison of the experimental values of S to the ones predicted by Hewitt [2]

T_w (°C)	α_{exp} (–)	X_{exp} (–)	S_{exp} (–)	S_{Hewitt} (–)
104.4	0.2025	0.944	680	6.9
108.9	0.229	0.1571	1040	7.8
113.2	0.2521	0.2395	1549	8.5
116.2	0.2428	0.2752	1963	8.2
120.3	0.2779	0.3479	2298	9.5
124.2	0.2008	0.4143	4668	6.8
128.8	0.1976	0.4838	6310	6.7
129.8	0.2141	0.4959	5986	7.3
139.5	0.1884	0.5431	8492	6.4
143.4	0.0874	0.5997	25942	3.6

surface and volume vapour fraction (Section 4.1) is not relevant and introduces a strong error. And an improved image analysis technique must be performed to take into account the thickness of the liquid film which is deposited either on the silicon or on the pyrex surfaces, and to measure the real volume vapour (or liquid) fraction.

The correlation proposed by Hewitt has been obtained with water and air and may therefore not be representative of a phase-changing system as in a boiling flow. Furthermore, this correlation has been elaborated in macro-systems where the surface/volume ratio is low and where surface effects are not as important as in micro-systems.

These criticisms show the difficulty in transposing correlations established in macro-systems to micro-systems where surface effects are more important.

5. Conclusion

The single phase heat transfer in laminar flow has here been observed to depend on the Reynolds number following a power law ($h = 6.96Re^2$), which is in fair agreement with the observations made by other researchers. The power observed here is higher than the one obtained by other authors, which may be due to the specific geometry.

The heat transfer coefficients obtained for a boiling flow are of the same order of magnitude as the ones obtained for the single phase heat transfer. Increasing the mass vapour fraction tends to reduce the heat transfer coefficient follow a power ($h_{boil} = 1452X^{-0.18}$), as shown by Agostini, even if the experimental values obtained in our experiments are lower than those obtained by both Agostini and Peng. The heat transfer coefficient appeared to be influenced by the Reynolds number, but only for Reynolds numbers below 12. At higher values there is no influence of the flow on the heat transfer. Moreover, the heat transfer coefficient tends to be strongly influenced by the wall temperature, whatever the flow conditions: the higher the wall temperature, the lower the heat transfer coefficient. This effect may be explained by the calefaction effect on the wall, described by the apparition of a vapour blanket between the wall and the liquid, which increases the thermal resistance of the system and therefore reduces the overall heat transfer coefficient.

Concerning the image analysis, the method we used needs to be improved to take into account the different types of contact between the liquid droplets and the channel walls: the assumption of equality between the surface vapour fraction measured and the real volume vapour fraction does not seem to be relevant. This study has also shown that gas–liquid flow, and especially vapour–liquid flow in boiling systems, are very complex. Additional work is required to characterize the micro-fluidic behaviour of such systems in order to better understand the thermal performances of micro-heat exchangers.

Acknowledgements

The research presented in this paper is funded by the European Union (project number: EU ENK6CT200000110).

References

[1] E.R. Delsman, E.V. Rebrov, M.H.J.M de Croon, J.C. Schouten, G.J. Kramer, V. Cominos, T. Richter, T.T. Veenstra, A. van den Berg, P.D. Cobden, F.A. de Bruijn, C. Ferret, U. d'Ortona, L. Falk, Mirth-e: micro reactor technology for hydrogen technology and electricity, in: Proceedings of the Fifth IMRET Conference, Strasbourg, 2001.
[2] G.F. Hewitt, Void fraction, in: G. Hetsroni (Ed.), Handbook of Multiphase Systems, McGraw-Hill, New York, 1982, Chapter 2.3.
[3] J. Brandner, M. Fitchner, U. Schygulla, K. Schubert, Improving the efficiency of micro heat exchangers and reactors, in: Proceedings of the Fourth IMRET Conference, Atlanta, 2000.
[4] C. Ferret, L. Falk, U. d'Ortona, M.N. Pons, T.T. Veenstra, F. Lim, A. van den Berg, Using image analysis to measure the heat transfer coefficient in a silicon micro-evaporator, in: Proceedings of Sixth IMRET Conference, New Orleans, 2002.
[5] H. Wensik, Fabrication of micro structures by powder blasting, Ph.D. Thesis, University of Twente, Enschede, The Netherlands, 2002.
[6] H.Y. Wu, P. Cheng, An experimental study of convective heat transfer in silicon micro-channels with different surface conditions, Int. J. Heat Mass Transf. 46 (2003).
[7] X.F. Peng, G.P. Peterson, Convective heat transfer and flow friction for water flow in micro channel structures, Int. J. Heat Mass Transf. 39 (1996).
[8] S. Garimella, W. Dowling, M.V.D. Veen, J. Killion, The effect of simultaneously developing flow on heat transfer in rectangular tubes, Heat Transf. Eng. 22 (2001).
[9] G. Tanda, Heat transfer in rectangular channels with transverse and V-shaped broken ribs, Int. J. Heat Mass Transf. 47 (2004).
[10] B. Agostini, Etude expérimentale de l'ébullition en convection force dans des mini-canaux, Ph.D. Thesis, Université Joseph Fourier, Grenoble, France, 2002.
[11] X.F. Peng, G.P. Peterson, B.X. Wang, Flow boiling of binary mixtures in micro channelled plates, Int. J. Heat Mass Transf. 39 (1995).
[12] K. Stephan, Heat transfer during boiling of pure substances in free convection, especially, in: Heat Transfer in Condensation and Boiling, Springer-Verlag, Berlin, 1992, Chapter 11, pp. 140–150.
[13] W.M. Rohsenow, General boiling, in: G. Hetsroni (Ed.), Handbook of Multiphase Systems, McGraw-Hill, New York, 1982, Chapter 6.1.
[14] N. Midoux, Mécanique et Rhéologis des fluids en Génie Chimique, Lavoisier Tech & Doc, 1993.